First-principles calculation of oxygen K-electron energy loss near edge structure of $HfO_2$



2009 J. Phys.: Condens. Matter 21 104212

(http://iopscience.iop.org/0953-8984/21/10/104212)

IOP PUBLISHING JOURNAL OF PHYSICS: CONDENSED MATTER

J. Phys.: Condens. Matter **21** (2009) 104212 (6pp) doi:10.1088/0953-8984/21/10/104212

# First-principles calculation of oxygen K-electron energy loss near edge structure of $HfO_2$

**T Mizoguchi**[1,4], **M Saitoh**[1,2] **and Y Ikuhara**[1,3]

[1] Institute of Engineering Innovation, The University of Tokyo, 2-11-16, Yayoi, Bunkyo, Tokyo 113-8656, Japan
[2] Device Platforms Research Laboratories, NEC Corporation, 1120, Shimokuzawa, Sagamihara, Kanagawa 229-1198, Japan
[3] Nano-structure Research Laboratory, Japan Fine Ceramics Center, Atsuta, Nagoya, Aichi 456-8587, Japan

E-mail: Mizoguchi@sigma.t.u-tokyo.ac.jp

Received 29 September 2008, in final form 30 October 2008
Published 10 February 2009
Online at stacks.iop.org/JPhysCM/21/104212

**Abstract**
Oxygen K-electron energy loss near edge structures (ELNES) of monoclinic, tetragonal, and cubic $HfO_2$ were calculated by the first-principles full-potential augmented plane wave plus local orbitals (APW + lo) method. By considering the relativistic effect as well as the core-hole effect in the calculation, the experimental oxygen K ELNES was successfully reproduced. The first, second, third, and fourth peaks originate from oxygen p components hybridized with Hf d-$e_g$, d-$t_{2g}$, s, and p components, respectively. It was found that the spectral differences among the polymorphs are mainly caused by the local structure of the Hf in the crystal.

## 1. Introduction

Oxides with a high dielectric constant ($k$) can be used to reduce the electrical thickness of a gate insulator without increasing the gate leakage current, and are expected to be necessary for further advanced complementary metal–oxide–semiconductor (CMOS) devices [1]. Thus, investigations of high-$k$ material properties have been performed from the viewpoint of microelectronic devices [2]. The great majority of recent studies on high-$k$ gate insulators have focused on hafnium oxide- ($HfO_2$-) based dielectrics because of their thermal stability, adequate conduction band and valence band offsets relative to Si, and high value of $k$ [3–5]. Recently, a $HfO_2$ gate insulator was actually employed in a state-of-the-art CMOS device [6], and the importance of $HfO_2$ gate insulators is increasing.

Since the dielectric properties of gate insulators are strongly affected by the composition and crystallinity of the gate oxide materials, understanding of the local structures in gate insulators is indispensable for further developments and improvements. However, the local structure analysis of gate insulators is always accompanied by difficulties due to their small thickness of a few nanometers. Among the analytical tools available, transmission electron microscopy (TEM) has been effectively used for gate insulator analysis owing to its high spatial resolution. In particular, electron energy loss spectroscopy (EELS) in conjunction with TEM has been used to investigate the atomic and electronic structures of the gate insulators [7–14].

The near edge structures of the EELS spectrum, namely electron energy loss near edge structures (ELNES), originate from the electron transition from a core orbital to unoccupied bands [15]. In the conventional transmission layout, only electronic transitions that are allowed by the electric dipole selection rule take place. The ELNES thereby reflects the partial density of state (PDOS) in the unoccupied bands, which can provide information on the atomic and electronic structures of the illuminated atoms. By combining EELS with modern scanning TEM (STEM), the spatial resolution of EELS can readily reach sub-nanometer scale, enabling atomic and electronic structure investigations with very high spatial resolution [16–18].

On the other hand, to extract atomic and electronic structure information from the ELNES, theoretical calculations are essential. In the theoretical calculations of ELNES reported

[4] Author to whom any correspondence should be addressed.

 

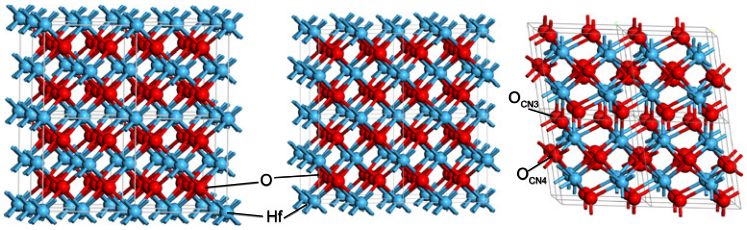


| | cubic-$HfO_2$ | tetragonal-$HfO_2$ | monoclinic-$HfO_2$ |
|---|---|---|---|
| Space group | $F_{m\bar{3}m}$ | $P_{42/nmc}$ | $P_{21/c}$ |
| Lattice constant | a=4.981Å | a=4.984Å<br>b=5.071Å | a=5.032Å γ=99.58°<br>b=5.125Å<br>c=5.192Å |

**Figure 1.** Crystal structure and crystallographic information for cubic, tetragonal, and monoclinic $HfO_2$. The structure and lattice constants of tetragonal $HfO_2$ are not those for a unit cell. The *a*-axis and *b*-axis of tetragonal $HfO_2$ are redefined as [1 1 0] and [$\bar{1}$ 1 0] of the conventional unit cell, respectively, so that the same number of atoms as that in the supercell of cubic and monoclinic $HfO_2$ can be treated. The two oxygen sites in monoclinic $HfO_2$ are named $O_{CN3}$ and $O_{CN4}$, which have threefold and fourfold coordination, respectively.

(This figure is in colour only in the electronic version)

so far [19–32], it has been clearly demonstrated that the inclusion of a core hole, i.e. an electronic hole on a core orbital associated with the electron transition process, is essential for reproducing the experimental spectra. The theoretical calculation of monoclinic-$HfO_2$ oxygen (O) K ELNES has been reported by McComb *et al*, and it was concluded that the first two peaks are caused by O p components hybridized with Hf d orbitals [11][5]. However, the other peaks in the spectrum were not assigned and ELNES calculations of other polymorphs have not been performed. In addition, although it is expected that the relativistic effect is important for calculating the electronic structure of $HfO_2$, the influence of the relativistic effect on the ELNES calculation of $HfO_2$ has not been discussed.

In this study, first-principles calculations of $HfO_2$ O K ELNES were performed. The influence of the relativistic effect as well as the core-hole effect on the calculation is discussed. In addition, to find relationships between the spectral features and the local atomic structure, O K ELNES for not only the monoclinic $HfO_2$ but also tetragonal and cubic $HfO_2$ were calculated. The spectral differences were investigated using the PDOS.

## 2. Methodology

The first-principles calculation of O K ELNES was performed by the full-potential augmented plane wave plus local orbital (APW + lo) method, WIEN2k code [33]. The generalized gradient approximation (GGA) proposed by Perdew *et al* [34] was employed for the exchange–correlation functional. All electrons up to 4d were treated as the core for Hf, while 1s electrons were treated as the core for oxygen. The muffin-tin radii, $R_{MT}$, for Hf and O were set to 2.1 and 1.6 Bohr, respectively. The product of the muffin-tin radius and the maximum reciprocal space vector $K_{max}$, i.e. the plane-wave cutoff, $R_{MT}K_{max}$, was fixed at 7.0 (Bohr $Ryd^{1/2}$). The maximum value of partial waves inside the atomic sphere was $\ell = 10$. Fully relativistic approximations were used for the core electrons. Regarding the valence and conduction bands, the relativistic effect is considered to be important because Hf is a heavy element. To determine the influence of the relativistic effect on the calculated results, non-relativistic, scalar-relativistic, and full-relativistic calculations were performed. In the full-relativistic calculation, spin–orbit coupling is fully considered.

It is known that $HfO_2$ has three types of polymorphs: monoclinic, tetragonal, and cubic. The crystal structures of these polymorphs are shown in figure 1. Their space groups are $F_{m\bar{3}m}$, $P_{42/nmc}$, and $P_{21/c}$, respectively. The unit cells of the monoclinic, tetragonal, and cubic structures have 12, 6, and 12 atoms, respectively. The lattice constants were determined by the first-principles projector augmented wave (PAW) method [35, 36] as implemented in the VASP code [37, 38]. This method was employed because of its efficiency and accuracy in structural optimization. The plane-wave cutoff energy was 500 eV and the *k*-point sampling meshes were set to 9 × 9 × 9, 13 × 13 × 9, and 9 × 9 × 9 for cubic-, tetragonal-, and monoclinic-$HfO_2$ primitive cells, respectively. The exchange–correlation functional was treated by the local density approximation (LDA) [39, 40]. It was confirmed that the calculated lattice constants are consistent with previously reported values [41–44]. Note that the calculated lattice constants are smaller than those obtained from experiments [45–47]. However, it was confirmed that the difference in the lattice constants of a few per cent does not affect the conclusions and discussion in this study.

One core hole was introduced at an oxygen 1s orbital. To reduce the interactions among the core holes due to the

[5] Although the authors did not mention about the relativistic effect, it is expected that a scalar relativistic calculation was performed, because the theoretical spectrum (figure 2 in this reference) is very similar to that calculated by considering the scalar relativistic effect in the present study.

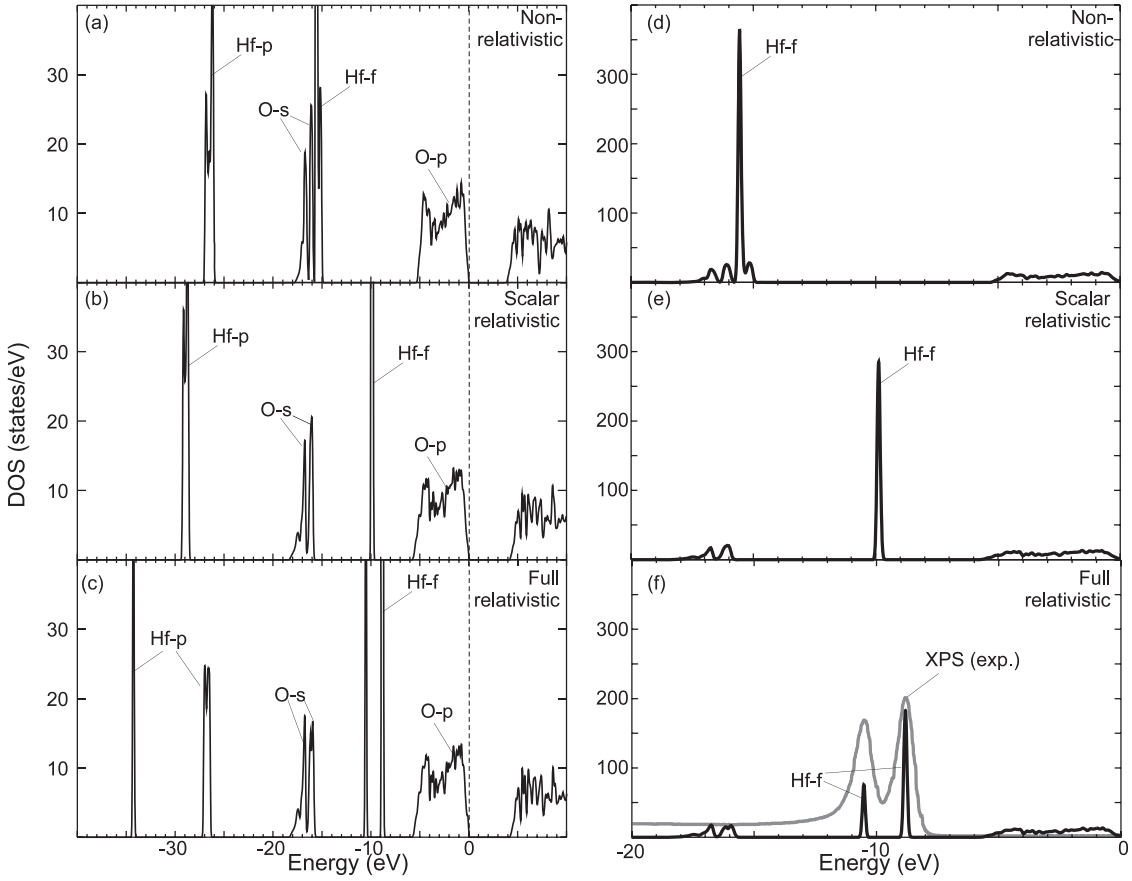


**Figure 2.** Density of states (DOS) of monoclinic $HfO_2$ calculated by (a) non-relativistic, (b) scalar-relativistic, and (c) full-relativistic calculation at the ground state. The XPS of Hf 4f and the corresponding DOS are compared in (d)–(f). The experimental XPS spectrum for monoclinic $HfO_2$ was obtained from [48]. The top of the valence band was set to zero.

three-dimensional periodic boundary conditions within the band structure calculations, they are replicated $2 \times 2 \times 2$, $2\sqrt{2} \times \sqrt{2} \times 2$, and $2 \times 2 \times 2$ times for the monoclinic, tetragonal, and cubic structures, respectively, and 96-atom supercells were constructed. Then, the excited atom with the core hole is more than 9.96 Å away from the adjacent excited atoms. Since monoclinic $HfO_2$ has two types of oxygen sites, $O_{CN3}$ and $O_{CN4}$, their O K ELNES were calculated separately, and the two O K edge spectra were added together with equal weighting to compare the total spectrum with the experimental spectrum.

The $k$-point sampling meshes used for self-consistent iterations and the ELNES calculation were $3 \times 3 \times 3$, $3 \times 3 \times 2$, and $3 \times 2 \times 2$ in the reciprocal space of the supercell for the monoclinic, tetragonal, and cubic structures, respectively. The spectral profile was obtained from the product of the radial part of the transition matrix element and the corresponding projected PDOS, which was broadened using a Gaussian function of $\Gamma = 1.0$ eV full width at half maximum. When the core hole was introduced, the transition energy was obtained from the difference between the total energy of the supercell at the ground and excited states.

## 3. Results and discussion

To find the importance of the relativistic effect in calculating the electronic structure of $HfO_2$, the density of states (DOS) of monoclinic $HfO_2$ was compared with the x-ray photoelectron spectroscopy (XPS) spectrum. Figure 2 shows the DOS obtained from non-relativistic, scalar-relativistic, and full-relativistic calculations, and the experimental XPS spectrum of the Hf 4f orbital [48]. The DOS was obtained from ground state calculation of a primitive cell of monoclinic $HfO_2$. Although Hf 4f and 5p orbitals are located at $-15$ eV and $-26$ eV in the non-relativistic calculation, they shift to $-10$ eV and $-29$ eV, respectively, in the scalar-relativistic calculation (figures 2(a) and (b)). In the full-relativistic calculation, the Hf orbitals split due to the spin–orbit coupling (figure 2(c)). By comparison with the experimental XPS spectrum, it is clear that only the full-relativistic calculation can reproduce the intensity and peak splitting (figures 2(d)–(f)). Similarly to the Hf orbitals, it is seen that the oxygen DOS is slightly changed by the relativistic effect because the oxygen orbitals hybridize with the Hf orbitals.

Here, the influence of the relativistic effect on the ELNES calculation is discussed. Since the experimental spectrum is obtained only from monoclinic $HfO_2$, the theoretical spectra of the monoclinic structure are first calculated. As mentioned above, the monoclinic structure has two types of oxygen sites, $O_{CN3}$ and $O_{CN4}$. The theoretical spectrum obtained from each site was separately calculated and aligned with the theoretical transition energy. The theoretical spectra calculated for different calculation conditions are compared in figure 3.

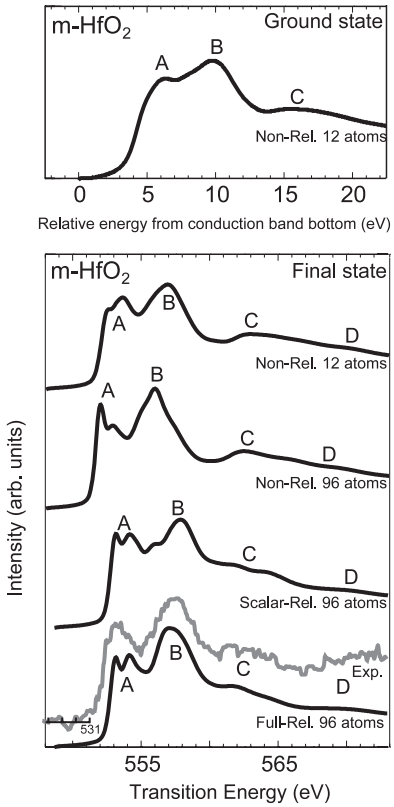


**Figure 3.** Calculated O K ELNES of monoclinic $HfO_2$ for different calculation conditions. The experimental O K ELNES for monoclinic $HfO_2$ was obtained from [9].

The calculated spectrum at the 'ground state' is also shown in the same figure. The ground state spectrum was obtained by calculating the transition matrix between the unoccupied bands and the core orbital, both of which are at the ground state. The calculated spectrum at the ground state has broad profiles of peaks A and B, whereas these peaks are apparent in the experiment. In the case of the non-relativistic calculation, even though a core hole was introduced in the 96-atom supercell, the splittings between peaks A–B and peaks B–C are respectively 3.5 eV and 6.5 eV, which are different from experiment, 4.5 eV and 4.2 eV. Better reproduction of the peak positions is obtained in the scalar-relativistic calculation. In the full-relativistic calculation, not only the peak position but also the peak intensity is well reproduced. It is concluded that inclusion of the relativistic effect as well as the core-hole effect are essential for the O K ELNES calculation of $HfO_2$.

O K ELNES for tetragonal and cubic $HfO_2$ were calculated and are compared with that of monoclinic $HfO_2$ in figure 4. Although the overall spectral profiles of cubic and tetragonal $HfO_2$ are very similar, upon detailed inspection we found the following four differences: (1) peak A of tetragonal $HfO_2$ is located 0.8 eV higher than peak A of cubic $HfO_2$, (2) the profile from peak A to peak B in tetragonal $HfO_2$ is slightly broader than that in cubic $HfO_2$, (3) peak C of tetragonal $HfO_2$ is less significant, and (4) peaks D and E of tetragonal $HfO_2$ are more significant than those in cubic $HfO_2$. Compared with the two polymorphs, the O K ELNES of monoclinic $HfO_2$ is located 0.2 eV higher than that of the tetragonal $HfO_2$, and has different spectral features; for example, peaks A and C in the monoclinic $HfO_2$ split and the profile between peak A and peak B is much broader than that of other polymorphs.

To find causes of these spectral differences, the PDOSs were investigated. Although the O K ELNES reflects the oxygen p-type PDOS, the cation components are dominant in the unoccupied bands, and the shape of the O K ELNES is strongly affected by the cation components [21, 49]. Hf and O PDOSs are shown in figure 4. From the PDOS diagrams, it was found that peaks A, B, C, and D in the three polymorphs commonly originate from the oxygen p component hybridized with Hf d-$e_g$, d-$t_{2g}$, s, and p components, respectively. The Hf PDOS in the tetragonal $HfO_2$ is very similar to that in the cubic $HfO_2$ but some peaks are slightly broader than that in the cubic $HfO_2$; for instance, Hf d-PDOS between 5 and 8 eV and Hf s- and p-PDOS. The broadening and splitting of PDOS is more significant in the monoclinic $HfO_2$. The Hf d-$e_g$ and d-$t_{2g}$ are overlapped with each other. From these PDOSs, it is found that the spectral differences among the polymorphs are related to the splitting and broadening of Hf PDOS in the unoccupied band.

These differences in the Hf PDOS can be ascribed to the different local symmetry of Hf in the crystal. Hf in cubic $HfO_2$ has octahedral coordination with $O_h$ point symmetry, resulting in clear peaks in PDOS and O K ELNES. Although the local symmetry is broken, the Hf retains its octahedral coordination in the tetragonal $HfO_2$. On the other hand, Hf in monoclinic $HfO_2$ has a more distorted structure with sevenfold coordination. Such distorted structures in monoclinic $HfO_2$ cause the peak splitting and broadening of PDOS and O K ELNES. This indicates that the spectral profiles of O K ELNES are sensitive to the local atomic structure of Hf in the crystal.

## 4. Summary

In this study, the O K ELNES of $HfO_2$, monoclinic, tetragonal, and cubic phases, were calculated by the first-principles full-potential APW + lo method. It was found that the relativistic effect as well as the core-hole effect is indispensable for the O K ELNES calculation of $HfO_2$. By considering the relativistic effect and the core-hole effect in the calculation, the experimental O K ELNES was successfully reproduced. From the PDOS analysis, it was found that the first to fourth peaks respectively originate from oxygen p components hybridized with Hf d-$e_g$, d-$t_{2g}$, s, and p components. It was found that the spectral differences among these polymorphs are caused by the local structure of the Hf site in the crystal.

In actual gate insulators, amorphous $HfO_2$ is partly formed and some additional elements, such as Si, N, and La, are intentionally/unintentionally present, and the presence of amorphous $HfO_2$ and the dopants strongly affects the dielectric properties. From this study, it was found that the spectral profiles in O K ELNES are sensitive to the local atomic structure. This conclusion strongly indicates that the combination of ELNES and the first-principles calculation has the potential to detect the local atomic and electronic structure changes caused by the amorphous $HfO_2$ and dopants in the

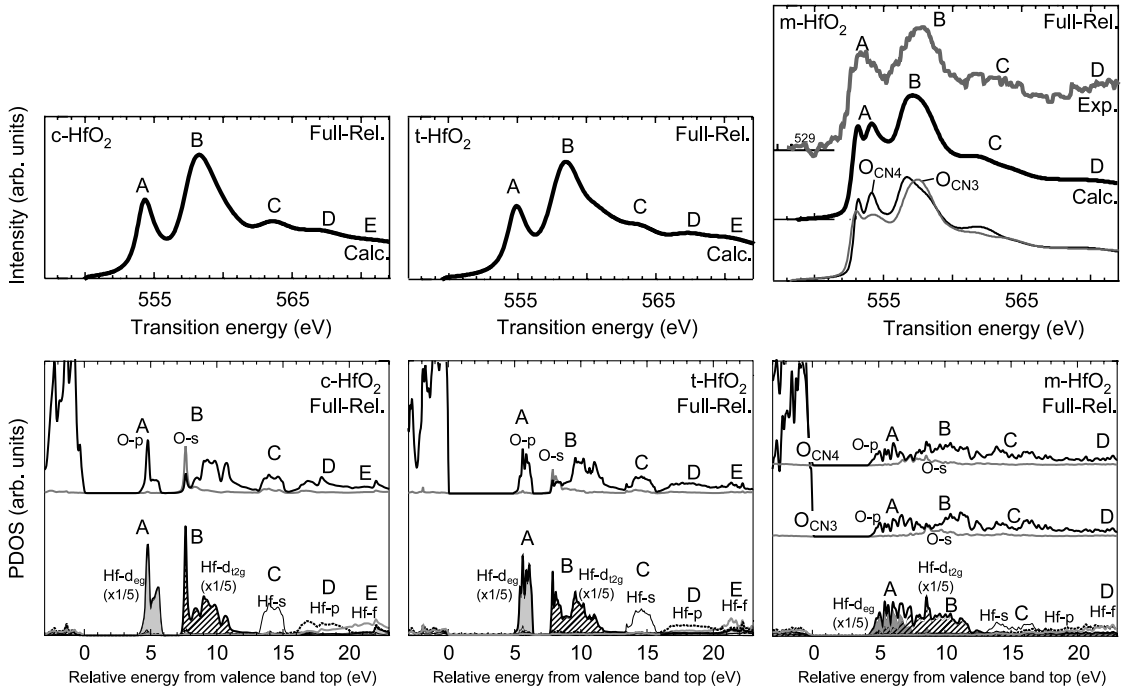


**Figure 4.** O K ELNES and PDOS of (left) cubic, (middle) tetragonal, and (right) monoclinic $HfO_2$. The experimental O K ELNES for monoclinic $HfO_2$ was obtained from [9].

gate insulators. The method established in this study, that is, inclusions of both the relativistic effect and the core-hole effect, is essential for the further analysis of such actual $HfO_2$ gate insulators.

## Acknowledgments

The authors acknowledge N Ikarashi at NEC Corp. and T Tohei, N Shibata, and T Yamamoto at the University of Tokyo for their helpful support and suggestions. This study was partially supported by a Grant-in-Aid for Scientific Research in Priority Area 'Nano Materials Science for Atomic Scale Modification 474' and Young Scientists (B) 20760449 from the Ministry of Education, Culture, Sports, Science, and Technology of Japan.

## References

[1] International Technology Roadmap for Semiconductors http://www.itrs.net/
[2] Wilk G D, Wallace R M and Anthony J M 2001 *J. Appl. Phys.* **89** 5243
[3] Robertson J 2000 *J. Vac. Sci. Technol.* B **18** 1785
[4] Saitoh M, Terai M, Ikarashi N, Watanabe H, Fujieda S, Iwamoto T, Ogura T, Morioka A, Watanabe K, Tatsumi T and Watanabe H 2005 *Japan. J. Appl. Phys.* **44** 2330
[5] Takeuchi H and King T J 2003 *Appl. Phys. Lett.* **83** 788
[6] Mistry K, Allen C, Auth C, Beattie B, Bergstrom D, Bost M, Brazier M, Buehler M, Cappellani A, Chau R, Choi C H, Ding G, Fischer K, Ghani T, Grover R, Han W, Hanken D, Hattendorf M, He J, Hicks J, Huessner R, Ingerly D, Jain P, James R, Jong L, Joshi S, Kenyon C, Kuhn K, Lee K, Liu H, Maiz J, Mclntyre B, Moon P, Neirynck J, Pae S, Parker C, Parsons D, Prasad C, Pipes L, Prince M, Ranade P, Reynolds T, Sandford J, Shifren L, Sebastian J, Seiple J, Simon D, Sivakumar S, Smith P, Thomas C, Troeger T, Vandervoorn P, Williams S and Zawadzki K 2007 *IEDM Tech. Dig.* 247
[7] Kimoto K, Matsui Y, Nabatame T, Yasuda T, Mizoguchi T, Tanaka I and Toriumi A 2003 *Appl. Phys. Lett.* **83** 4306
[8] Ikarashi N, Miyamura M, Masuzaki K and Tatsumi T 2004 *Appl. Phys. Lett.* **84** 3672
[9] Craven A J, MacKenzie M, McComb D W and Docherty F T 2005 *Microelectron. Eng.* **80** 90
[10] Agustin M P, Bersuker G, Foran B, Boatner L A and Stemmer S 2006 *Appl. Phys. Lett.* **100** 24103
[11] McComb D W, Craven A J, Hamilton D A and Mackenzie M 2004 *Appl. Phys. Lett.* **84** 4523
[12] Ikarashi N, Watanabe K, Masuzaki K, Nagkagawa T and Miyamura M 2006 *J. Appl. Phys.* **100** 063507
[13] Mackenzie M, Craven A J, Hamilton D A and McComb D W 2006 *Appl. Phys. Lett.* **88** 022108
[14] Jang J, Park T J, Kwon J H, Jang J H, Hwang C S and Kim M 2008 *Appl. Phys. Lett.* **92** 232906
[15] Egerton R F 1996 *Electron Energy-Loss Spectroscopy in the Electron Microcopy* (New York: Plenum)
[16] Varela M, Findlay S D, Lupini A R, Christen H M, Borisevich A Y, Dellby N, Krivanek O R, Nellist P D, Oxley M P, Allen L J and Pennycook S J 2004 *Phys. Rev. Lett.* **92** 95502
[17] Kimoto K, Aasaka T, Nagai T, Saito M, Matsui Y and Ishizuka K 2007 *Nature* **450** 702
[18] Mizoguchi T, Varela M, Buban J P, Yamamoto T and Ikuhara Y 2008 *Phys. Rev.* B **77** 024504
[19] Tanaka I and Adachi H 1996 *Phys. Rev.* B **54** 4604
[20] Tanaka I, Araki H, Yoshiya M, Mizoguchi T, Oba F and Adachi H 1999 *Phys. Rev.* B **60** 4944
[21] Mizoguchi T, Tanaka I, Yoshiya M, Oba F, Ogasawara K and Adachi H 2000 *Phys. Rev.* B **61** 2180
[22] Lie K, Høier R and Brydson R 2000 *Phys. Rev.* B **61** 1786

[23] Mo S D and Ching W Y 2000 *Phys. Rev.* B **62** 7901
[24] Mo S D and Ching W Y 2001 *Appl. Phys. Lett.* **78** 3809
[25] Elsässer C and Köstlmeier S 2001 *Ultramicroscopy* **86** 325
[26] Nufer S, Gemming T, Elsässer C, Köstlmeier S and Rühle M 2001 *Ultramicroscopy* **86** 339
[27] Hébert C 2007 *Micron* **38** 12
[28] Mizoguchi T, Tanaka I, Yoshioka S, Kunisu M, Yamamoto T and Ching W Y 2004 *Phys. Rev.* B **70** 45103
[29] Yamamoto T, Mizoguchi T and Tanaka I 2005 *Phys. Rev.* B **71** 245113
[30] Tanaka I, Mizoguchi T and Yamamoto T 2005 *J. Am. Ceram. Soc.* **88** 2013
[31] Ching W Y and Rulis P 2008 *Phys. Rev.* B **77** 035125
[32] Ching W Y, Ouyang L Z, Rulis P and Yao H Z 2008 *Phys. Rev.* B **78** 014106
[33] Blaha P, Schwarz K, Madsen G, Kvasicka D and Luitz J 2001 *WIEN2k, An Augmented Plane Wave+Local Orbitals Program for Calculating Crystal Properties* Techn. Universitat Wien Austria ISBN 3-9501031-1-2, Karlheinz Schwarz
[34] Perdew J P, Burke K and Ernzerhof M 1996 *Phys. Rev. Lett.* **77** 3865
[35] Blöchl P E 1994 *Phys. Rev.* B **50** 17953
[36] Kresse G and Joubert D 1999 *Phys. Rev.* B **59** 1758
[37] Kresse G and Hafner J 1993 *Phys. Rev.* B **47** R558
[38] Kresse G and Furthmüller J 1996 *Phys. Rev.* B **54** 11169
[39] Ceperley D M and Alder B J 1980 *Phys. Rev. Lett.* **45** 566
[40] Perdew J P and Zunger A 1981 *Phys. Rev.* B **23** 5048
[41] Kang J, Lee E C and Chang K J 2003 *Phys. Rev.* B **68** 054106
[42] Zhao X and Vanderbilt D 2002 *Phys. Rev.* B **65** 233106
[43] Mukhopadhyay A B, Sanz J F and Musgrave C B 2006 *Phys. Rev.* B **73** 115330
[44] Zheng J X, Ceder G, Maxisch T, Chim W K and Choi W K 2007 *Phys. Rev.* B **75** 104112
[45] Wang J, Li H P and Stevens R 1992 *J. Mater. Sci.* **27** 5397
[46] Adams D M, Leonard S, Russel D R and Cernik R J 1991 *J. Phys. Chem. Sol.* **52** 1181
[47] Stacy D W, Johnstone J K and Wilder D R 1972 *J. Am. Ceram. Soc.* **55** 482
[48] Chastain J and King R C Jr 1995 *Handbook of X-Ray Photoelectron Spectroscopy* (Eden Prairie, MN: Physical Electronics)
[49] Mizoguchi T, Tatsumi K and Tanaka I 2006 *Ultramicroscopy* **106** 1120